RSC Advances

ROYAL SOCIETY OF CHEMISTRY

www.rsc.org/advances

Cite this: DOI: 10.1039/c0xx00000x

ARTICLE TYPE

www.rsc.org/advances

The inelastic electron tunneling spectroscopy of curved finite-sized Graphene nanoribbon based molecular devices

Zongling Ding,*[a,b] Zhaoqi Sun[a], Guang Li[a], Fanming Meng[a], Mingzai Wu[a], Yongqing Ma[a] and Xiaoshuang Chen[c]

Received (in XXX, XXX) Xth XXXXXXXXX 20XX, Accepted Xth XXXXXXXXX 20XX
DOI: 10.1039/b000000x

The inelastic electron scattering properties of the molecular devices of curved finite-sized graphene nanoribbon (GNR) slices have been studied by combining the density functional theory and Green's function method. Based on the extended molecular models, the inelastic electron tunneling spectroscopy, inelastic quantum conductance and inelastic current have been calculated systematically. The temperature dependences of the inelastic electron tunneling spectroscopy (IETS) and inelastic current have been discussed. Results show that the contributions of the inelastic conductance increase obviously and become comparable to the elastic conductance for curved GNR slices based junctions. The electron inelastic scattering of the curved GNR-based junctions are orders of magnitude stronger than that of the plane ones. The obvious dependences of the elastic and inelastic current of the finite-sized GNR slices make it have probable applications in molecular microprobes.

Introduction

Due to the remarkable structural, electrical and chemical properties, graphene based low-dimensional carbon materials have been widely studied both on theoretically and experimentally grounds [1-6]. In addition to the unique electronic properties, graphene sheets also have very good flexibility and mechanical properties. Graphene and related materials are ideally suited for applications in flexible and plastic electronics [7-10]. Meanwhile, with the development of experimental method, people can prepare, characterize and control extremely small scale systems even a single molecule. For practical applications, nano-scale molecular devices based on extremely small graphene nanoribbon (GNR) sheets become possible. The electronic properties of graphene nano-scale sheets are strongly dependent on their geometry [11]. The electronic properties of curved graphene nano-scale sheets are considerably different from those of their plane counterparts. It is worth mentioning that the flexible touch screen panels [12] of graphene have been indeed realized. In practical applications, the curvature dependence of elastic and inelastic current for the finite-sized GNR based junctions makes it have probable applications in molecular microprobes.

Inelastic electron tunneling spectroscopy (IETS) was developed in the 1960s to study vibrational spectra of organic molecules buried inside metal-oxide-metal junctions and has since become a powerful spectroscopic tool for molecular identification and chemical bonding investigations [13–20]. There are many significant theoretical works on the topic of IETS have been reported [21-25].The inelastic tunneling process is induced by the coupling between the atom motion and electrons, thus the inelastic transport properties of molecular devices are very sensitive to the configuration. In addition, IET process is closely related to the molecular energy level, molecular motion, the charge transfer and chemical reaction process. It is known that the inelastic component can lead to a second tunneling path, which gives an additional current contribution to the tunneling current if the transmission is far below unity. While in case of a close to unity transmission the inelastic current can reduce the current (have a negative sign) by producing a "dip" in the IET spectrum. Generally, the inelastic contribution to the current is small compared to the elastic tunneling current and is more clearly seen as a peak in the second derivative of the current to the bias voltage. Investigations with IETS have had significant technological implications because they give structural information about the molecular junction and provide a direct access to the dynamics of energy relaxation and thermal dissipation during the electron tunneling. Therefore, the studied of the effect of curvature on the elastic and inelastic electronic and transport properties of graphene nanoscale sheets is necessary.

Theory and Calculation methods

The calculations of geometric optimization and electronic properties are performed by the density functional theory in B3LYP level [26, 27]. Mixed basis set have been used, that is, using the 6-31G basis set for carbon and hydrogen atoms and LanL2DZ basis set for Au atoms. The elastic and inelastic transport

properties are carried out using the quantum chemistry for molecular electronics (QCME) code [28-30]. The approach for both elastic and inelastic scattering is based on scattering theory and Green's functional theory. The finite-sized GNR based molecular device was decomposed into three parts, the source, the drain and the extended molecule. When energetic constraints are satisfied, the electron crossing the junction may exchange a definite amount of energy with the molecular nuclear motion, resulting in an inelastic component in the transmission current [31]. To describe the electron-vibronic coupling effect, molecular theory based on vibrational normal modes has been introduced to the scattering model. In the adiabatic Born-Oppenheimer approximation, the purely electronic Hamiltonian of the molecular systems can be considered parametrically as dependent on the vibrational normal modes Q. Therefore, the total electron tunneling current (I) in the junctions include the contributions of elastic (I_{el}) and inelastic (I_{inel}) electron scattering from the source to drain electrode.

$$I = I_{el} + I_{inel} \qquad (1)$$

Typically, only a fraction of tunneling electrons has involved in the inelastic tunneling process. The small conductance change induced by the electron-vibronic coupling is commonly measured by the second harmonics of a phase-sensitive detector for the second derivative of the tunneling current d^2I/dV^2 or the part normalized by the differential conductance $(d^2I/dV^2)/(dI/dV)$.

By using a Taylor expansion, the nuclear motion depended wavefunction can be expanded along each vibrational normal mode. Since most IETS are measured at the electronic off-resonant region (that is, conducting levels are far from the Fermi energy), the adiabatic harmonic approximation can be applied. We can then use the first derivative to represent the vibrational motion part in the wavefunctions. In this case, the total quantum conductance is described as

$$\sum_{\nu',\nu,\nu''} g_{K'K}^{\eta,\nu',\nu,\nu''} = \sum_{\alpha} \frac{1}{z_\eta - \varepsilon_\eta - \hbar\omega_\alpha} \times \sqrt{\frac{\hbar}{2\omega_\alpha}} \times [\left\langle K_0'^{\eta} \left| \frac{\partial \Psi_0^{\eta}}{\partial Q_\alpha} \right\rangle + \left\langle \frac{\partial K_0'^{\eta}}{\partial Q_\alpha} \right| \Psi_0^{\eta} \right\rangle] \times [\left\langle K_0^{\eta} \left| \frac{\partial \Psi_0^{\eta}}{\partial Q_\alpha} \right\rangle + \left\langle \frac{\partial K_0^{\eta}}{\partial Q_\alpha} \right| \Psi_0^{\eta} \right\rangle] \qquad (2)$$

where ε_η represent the energy of eigenstate η of the pure electronic Hamiltonian, ω_α is the vibrational frequency of vibrational normal modes Q_α, and n_α^ν is the quantum number for the mode Q_α in the vibration wavefunction $|\Psi^\nu(Q)\rangle$. Ψ_0^η is here the intrinsic electronic wavefunction at the equilibrium position, Q_0. The parameter z in the Green's function is a complex variable $z = E_i + i\Gamma_i$ and E_i is the energy at which the scattering process is observed. Γ_i is the escape rate. The electrodes of molecular devices often contain huge numbers of metal atoms, the vibrational information usually shadowed in the free electron gas environment. Generally the electron-vibronic coupling can be obviously observed and discussed only in the extended molecule part [32]. Thus, the eigenstate at energy level ε_η can be partitioned into three parts runs over the atomic sites in the molecule: the source, drain and extended molecule. The term $|K^\eta\rangle$ is the wave function of the extended molecule subsystem. From equation (2) one can see that considering molecular vibrations in the wave function and the Hamiltonian will introduce vibrational excited states on the basis of ground state of the system. In the off-resonance region, the scattering of electrons from these states will contribute some inelastic electron tunneling.

Results and Discussions

Models

In this article, a series of Au(111)-4×4-extended-molecule-Au(111) junctions with different distances between the source and drain electrodes (d_{SD} from 1.37 nm to 1.77 nm) have been considered as the model systems. A concise figure of the molecular devices is given in figure 1. The 4×4 prototype graphene nanoribbon slice with 8 carbon atoms on the zigzag (ZZ) edges and 8 carbon atoms on the armchair (AC) edges as the basic molecular core. All of the dangling edge carbon atoms on the both sides of ZZ and AC edges have been passivated by Hydrogen atoms. The extended molecules are composed of GNRs sandwiched between triangle gold clusters. The introductions of a large number of metal atoms in the system often bring magnitude growth of the quantum chemistry calculations. Furthermore, the main and most important IETS information comes from the vibrations of the molecule atoms and the vibration of electrode metal atoms almost have no effect on the IETS spectra of the device. Therefore, we choose triangle gold clusters composed of three gold atoms to describe source and drain electrodes of the extended molecules. In the geometry optimization process, the coordinate of the Au atoms have been fixed and the atoms of molecular core are fully optimized. We have studied systematically on the effect of fixed electrodes on the geometric and transport properties of GNR slices based molecular devices in one of our previous work [33]. The results shown that with different d_{SD}, the central atomic plane exhibited different degrees of curvature. Here, we are mainly interested in the effect of curvature on the inelastic tunneling spectroscopy of finite-sized GNR slices based junctions. It is worth mentioning that for the junction models Au atoms are connected with the molecular core through hydrogen atoms. This actually has a large contact resistance. Therefore, if one choose other atoms with small contact resistance (such as sulphur atom), the conductance should increase significantly.

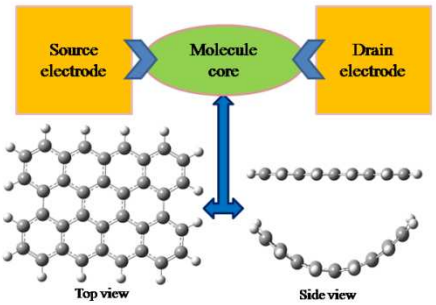

Figure 1. Structures of the 4×4 GNR based molecular junctions.

The elastic and inelastic quantum conductances of curved 4x4GNRs-based junctions

It is known that in the nanomolecular devices, electrons scatter from the ground state in the source reservoir to an excitation level, and transport through the conducting channel to the ground state in the drain reservoir. The molecular orbitals of the extended molecule serve as the conducting channels. The inclusion of nuclear motion introduces vibrational excited states in the electronic ground state potential. These vibrational excited states are the ones that contribute to the inelastic terms in the case of off-resonant excitation. Meanwhile, the electron can also tunnel through the molecular orbitals, resulting in the elastic term in the total current. Therefore, the total quantum conductance in the junctions can be divided into two parts, the elastic and inelastic electron scattering from source to drain electrodes. The calculated elastic and inelastic quantum conductance (here, we plot as G/G_0 with $G_0=2e^2/h$ being the conductance quantum, bias voltage=2V, at room temperature) curves of a series of 4×4 GNR-based molecular devices with different d_{SD} and curvature radius have been given in figure 2. The black solid lines are for the elastic and red dashed lines are for the inelastic conductance.

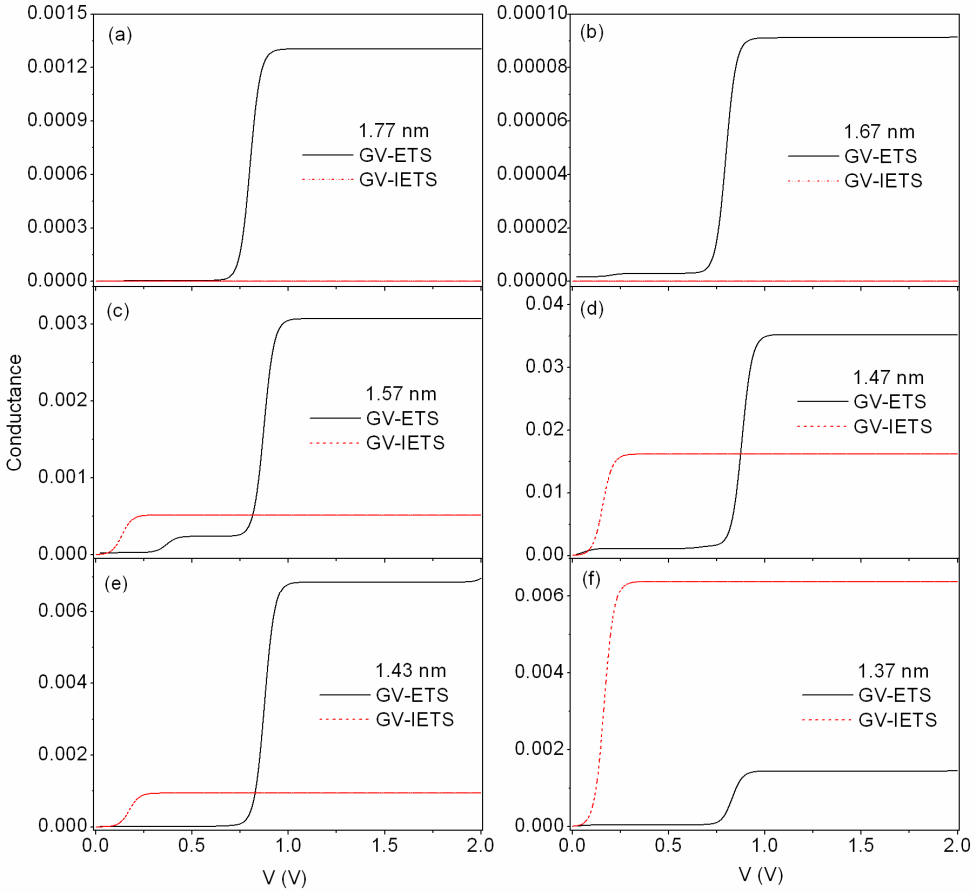

Figure 2. The elastic and inelastic quantum conductance (plot as G/G_0 with $G_0=2e^2/h$ being the conductance quantum, bias voltage=2V) curves of curved 4×4 GNR-based junctions with different d_{SD}.

From figure 2 one can clearly see that the intensity of quantum conductance is sensitive to the atom structure of central molecular core, while the positions of quantum conductance stairs appear at same energy region. Based on the junction models, the coordinate of the Au atoms have been fixed (that is, there is a certain d_{SD} for each system) and the atoms of molecular core are fully relaxed in the geometry optimization process. Our previous results obtained that the curvature radius of the atomic plane is increased, and the deformation energy is decreased with the stretching of d_{SD}. When d_{SD} is larger than 1.67 nm, the curvature radius becomes very large and the deformation energy keeps as a constant [33]. Comparing with the elastic conductance, the contributions of the inelastic conductance increase obviously when d_{SD} decreasing. The inelastic conductance can be negligible for the large d_{SD} systems (plane GNR slices) as shown in figure 2(a) and (b). For the small d_{SD} systems (curved GNR slices), the contributions of inelastic conductance become comparable to the elastic conductance, as shown in figure 2(c) to (e). It is need to mention that the main contribution for the total conductance comes from the inelastic electron scattering in systems with small curvature radius, such as d_{SD}=1.37nm system shown in figure 2(f). The reason may that the curvature of the GNR slices causes the hybridization of the electrons changed, and the nuclear motion for the curved systems is much stronger than that of the plane systems. The nuclear motion can introduces vibrational excited states which contribute to the inelastic electron scattering. These two mechanisms can tune the molecular orbitals and thus change the quantum conductance. From figure 2, one also sees that there are some differences on the magnitude of conductance. Fixed the coordinate of source drain electrodes in the

optimization process, equivalent to apply stress to the GNR plane, which cause the atomic plane become curved, thus the electronic properties of the system and the transport properties of the junctions will be tuned. Furthermore, the coupling between electrodes and molecule core will also have effect on the transport properties. The proportion of elastic and inelastic component of the total current can provide a referential reflection of the localized curvature information for the GNR slices.

The inelastic electron tunneling spectroscopy of curved 4x4GNRs-based junctions

Inelastic electron tunneling spectroscopy is a powerful spectroscopic tool for molecular identification and chemical bonding investigations. In this part, we studied the inelastic electron scattering properties of several 4x4 GNR-based molecular devices. The calculated IETS (d_{SD} from 1.37nm to 1.77nm) are illustrated as a function of applied bias in figure 3. The shape of the calculated IETS curve agrees well with each other, while the peak positions are different. Generally, the amplitude of the IETS peak for the curved GNR-based junctions has blue-shift with decreasing the d_{SD}. That is, with the atomic plane become more curved, vibrational energy states appear at larger energy region. With the d_{SD} become smaller, the curvature radius become smaller and the coupling between Au atoms and carbon atoms become stronger. When the d_{SD} become much smaller, the strong coupling may constraint the nuclear motion partially, thus, the blue-shift effect cannot be seen for the d_{SD}=1.37nm system. For the d_{SD}=1.77nm system, the molecular core keeps plane atomic structure and the overlap between Au atoms and edge passivated hydrogen atoms and sub-edge carbon atoms can be negligible. There are a quite small IETS peak appears at low energy regions. One can conclude that the electron inelastic scattering of the curved GNR-based junctions are orders of magnitude stronger than that of the plane ones. The large difference in the spectral intensity and distributions related to the molecular vibrational modes implies that the molecular conformations and the connection of molecular core and electrodes are different.

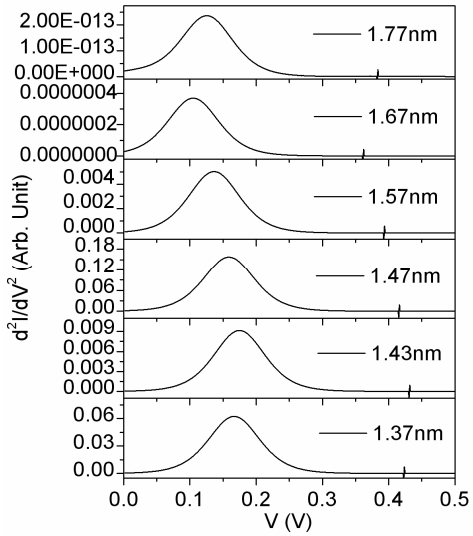

Figure 3. The inelastic electron tunneling current as function of source-drain bias voltage of the curved GNR-based molecular devices with different d_{SD}.

The temperature dependences of inelastic electron scattering for curved 4x4GNRs-based junctions

As we all know, temperature have a profound impact on the electron scattering process. Based on the theoretical calculation methods used by the QCME code, we can find that there are two main factors closely related to temperature, one is the population distribution of thermal particles (the molecular vibrational mode has been used to describe the atomic motion in this method) which can be calculated using the Boltzmann distribution function P_n. The other is the electron Fermi distribution at the end of source and drain electrodes f(E), where

$P_{n_\alpha^{V''}} = e^{-[\Delta E/k_B T]}$, source $f(E) = \frac{1}{e^{[(E-E_f)/k_B T]}+1}$ and drain $f(E) = \frac{1}{e^{[(E-E_f-eV_D)/k_B T]}+1}$.

Both of the two factors have exponential dependence on temperature. The effect of Boltzmann distribution function on the tunneling current is only valid in the low frequency range. For the Fermi distribution, the energy difference is often close to zero in the vicinity of the conducting orbits, thus the effect of Fermi distribution on the tunneling current is persistent.

In order to examine the dependence of the IETS on the temperature, we choose two extended molecules with d_{SD}=1.57nm and d_{SD}=1.77nm as example for simplicity. The calculated inelastic electron tunneling spectroscopy under different working temperatures for the d_{SD}=1.57nm system and inelastic electron tunneling current (on a log scale) under different temperature for the d_{SD}=1.57nm and d_{SD}=1.77nm system are shown in figure 4, respectively. Our calculated results shown that there is a peak of IETS in the low-frequency regions below 50mV for curved-GNR based systems. The intensity of this peak is very small. While for the plane-GNR based systems with a large value of d_{SD}, the molecular vibrational level appear until 100mV. It can be seen that the IETS curve of d_{SD}=1.57nm

system have significant temperature dependence between 100mV and 200mV. From figure 4 (a) to (f), one can see that the peak has a significant broadening with the increase of temperature. Figure 4 (g) shows that in the low-frequency region below 50mV, the inelastic current curve for the d_{SD}=1.57nm system is very insensitive to temperature. There are obvious changes of the inelastic current curves near 140mV for the d_{SD}=1.57nm and d_{SD}=1.77nm systems as shown in figure 4 (g) and (h). Due to the influence of molecular vibrational modes, a new conductance level has been introduced. With the increasing of temperature, the spectral width becomes lager and lager. Until a certain temperature, the fine structure of the spectroscopy will be covered up. The high-frequency vibration modes are mainly from the contribution of the molecules. The metal atoms considered in the extended molecules will bring many low frequency vibration modes which usually derived from the metal atoms or metal-molecule vibration. In the low-energy region, the population distribution of thermal particles has a strong effect even at low temperatures. Almost all of the vibration information will be shadowed. Thus, the changes of inelastic current below 50mV for the d_{SD}=1.77nm system as shown in figure 4 (h) are mainly caused by the population distribution of thermal particles. One can thus conclude that the effect of temperature dependence of population distribution of thermal particles is relatively obvious in the low-frequency area. And the temperature dependence effect of IETS is mainly introduced by the Fermi distribution function. The difference in the spectral intensity distribution and temperature dependence related to the molecular vibrational modes implies that the molecule-electrodes coupling and degree of curvature of the two systems are different. It is necessary to mention that when the curvature of the GNR slice become very large such as the d_{SD}=1.37nm system, the inelastic scattering become much high, the equilibrium distributions assumption should be corrected and developed. The local thermodynamic equilibrium assumption still can be used for the contacts, while for the molecular core of the junction the effect of proper non-equilibrium phonon population needs to be considered [34].

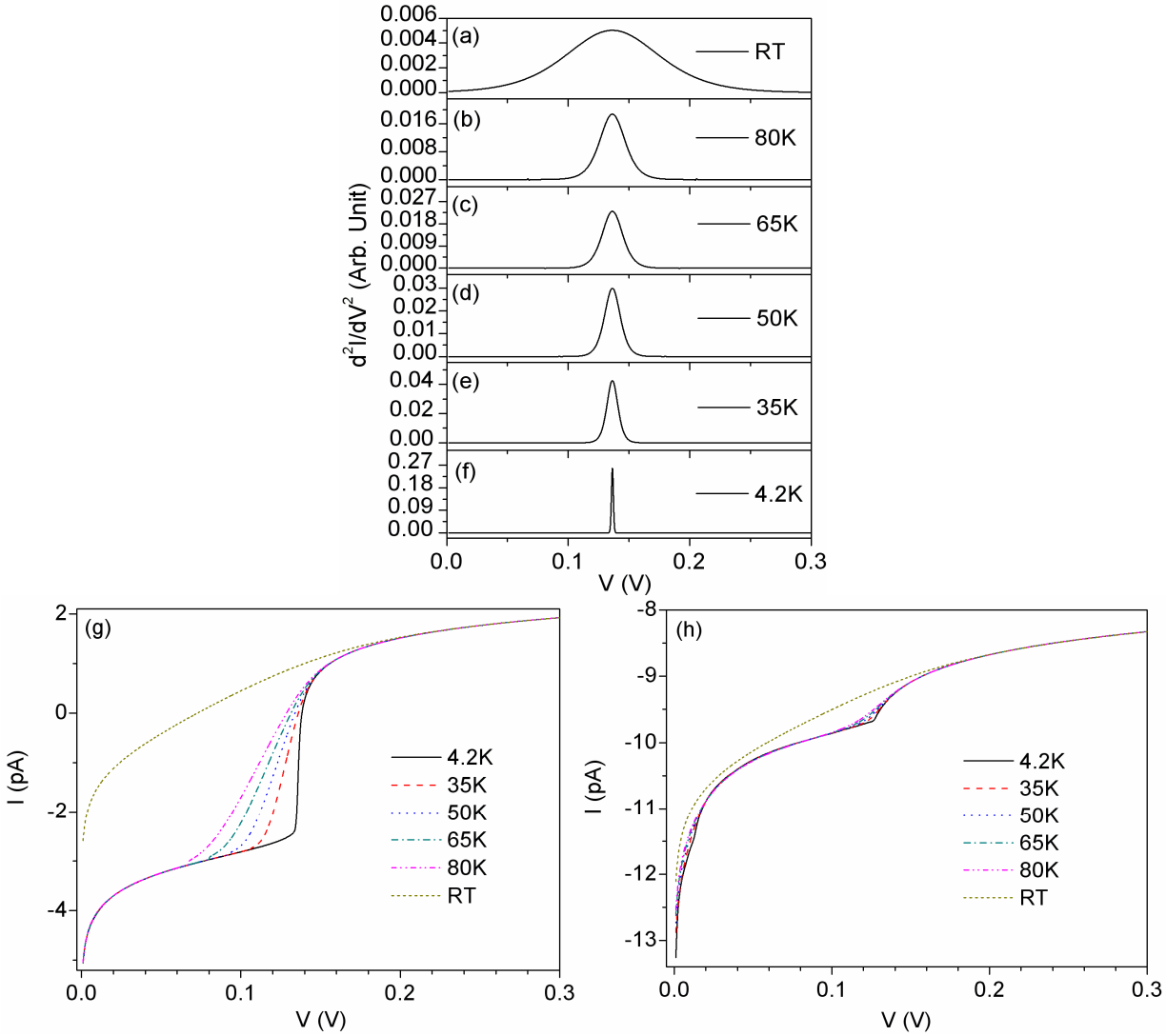

Figure 4. (a)-(f) The inelastic electron tunneling spectroscopy under different working temperatures for the d_{SD}=1.57nm system,. (g), (h) Calculated inelastic electron tunneling current (on a log scale) under different working temperature for the d_{SD}=1.57nm and d_{SD}=1.77nm system, respectively.

Conclusions

In this paper, the 4×4 finite-sized GNR slices are chosen as the

prototype structure. In order to understand how the effect of curvature and temperature on the electronic structure and inelastic transport properties of finite-sized curved-GNR slices, several junctions with different d_{SD} have been considered. We focus on the electron inelastic tunneling spectroscopy. Comparing with the elastic conductance, the contributions of the inelastic conductance increase obviously when d_{SD} increasing. The inelastic conductance can be negligible for plane GNR slices based junctions. For the curved GNR slices based junctions, the contributions of inelastic conductance become comparable to the elastic conductance. The electron inelastic scattering of the curved GNR-based junctions are orders of magnitude stronger than that of the plane ones. The effect of temperature dependence of population distribution of thermal particles is relatively obvious in the low-frequency area. And the temperature dependence effect of IETS is mainly introduced by the Fermi distribution function. From practical applications point of view, for one hand the curvature and temperature dependence of the elastic and inelastic current for the finite-sized GNR based junctions can provide a referential reflection of the localized curvature information for the GNR slices, for the other it have probable applications in molecular microprobes.

Acknowledgments

This work was supported in part by the National Natural Science Foundation of China (11304001, 51272001, 51472003 and 11174002), the National Key Basic Research Program (2013CB632705), the Ph.D. Programs Foundation for the Youth Scholars of Ministry of Education of China (20133401120002), the Foundation of State Key Laboratory for Modification of Chemical Fibers and Polymer Materials Donghua University (LK1217), the Foundation of Co-operative Innovation Research Center for Weak Signal-Detecting Materials and Devices Integration Anhui University (01001795-201410), the Key project of the Foundation of Anhui Educational Committee (KJ2013A035) and the Ph.D. Programs Foundation of Anhui University (33190134). Computational resources from the Shanghai Supercomputer Centre are acknowledged.

Notes and references

[a] *School of Physics and Material Science, Anhui University, Jiu Long Road 111, Hefei, China, 230601. Fax: +86-551- 6386 1257; Tel: +86-551-6386 1257; E-mail: zlding@ahu.edu.cn*

[b] *Co-operative Innovation Research Center for Weak Signal-Detecting Materials and Devices Integration, Anhui University, Jiulong Road NO.111, Hefei, China, 230601*

[c] *National Lab. of Infrared Physics, Shanghai Institute for Technical Physics, Chinese Academy of Sciences, Yu Tian Road 500, Shanghai, China, 230083. Fax: +86-21-6583 0734; Tel: +86-21-3505 2062; E-mail: xschen@mail.sitp.ac.cn*

1 Y. Q. Xue, M. A. Ratner, *Phys. Rev. B* **2004**, *69*, 085403(1)-085403(5).
2 R. Cohen, K. Stokbro, J. M. L. Martin, M. A. Ratner, *J. Phys. Chem. C* **2007**, *111*, 14893-14902.
3 Y. Xu, Z. Lin, X. Huang, Y. Liu, Y. Huang, X. Duan, *ACS Nano* **2013**, *7*, 4042-4049.
4 S. W. Seo, E. Jung, S. J. Seo, H. Chae, H. K. Chung, S. M. Cho, *J. Appl. Phys.* **2013**, *114*, 143505(1)-143505(7).
5 X. W. Wang, G. Z. Sun, P. Routh, D. H. Kim, W. Huang, P. Chen, *Chem. Soc. Rev.* **2014**, *43*, 7067-7098.
6 K. S. Mali, J. Greenwood, J. Adisoejoso, R. Phillipson, S. D. Feyter, *Nanoscale* **2015**, *7*, 1566-1585.
7 Y. H. Wang, K. Bian, C. G. Hu, Z. P. Zhang, N. Chen, H. M. Zhang, L. T. Qu, *Electrochem. Commun.* **2013**, *35*, 49-52.
8 S. Das, P. Sudhagar, Y. S. Kang, W. Choi, *J. Mater. Res.* **2014**, *29*, 299-319.
9 J. H. Lee, J. Y. Tan, C. T. Toh, S. P. Koenig, V. E. Fedorov, A. H. C. Neto, Ozyilmaz B., *Nano Lett.* **2014**, *14*, 2677−2680.
10 M. A. Bissett, M. Tsuji, H. Ago, *Phys. Chem. Chem. Phys.* **2014**, *16*, 11124-11138.
11 H. H. Pu, S. H. Rhim, C. J. Hirschmug, M. Gajdardziska-Josifovska, M. Weinert, J. H. Chen, *Phys. Rev. B* **2013**, *87*, 085417(1)-085417(6).
12 K. S. Kim, Y. Zhao, H. Jang, S. Y. Lee, J. M. Kim, K. S. Kim, J. H. Ahn, P. Kim, J. Y. Choi, B. H. Hong, *Nature Lett.* **2009**, *457*, 706-710.
13 J. G. Kushmerick, J. Lazorcik, C. Patterson H., R. Shashidhar, D. S. Seferos, G. C. Bazan, *Nano. Lett.* **2004**, *4*, 639-642.
14 W. Wang, T. Lee, I. Kretzschmar, M. A. Reed, *Nano. Lett.* **2004**, *4*, 643-646.
15 L. H. Yu, Z. K. Keane, J. W. Ciszek, L. Cheng, M. P. Stewart, J. M. Tour, D. Natelson, *Phys. Rev. Lett.* **2004**, *93*, 266802(1)-266802(4).
16 A. H. Flood, J. F. Stoddart, D. W. Steuerman, J. R. Heath, *Science*, **2004**, *306*, 2055-2056.
17 J. Jiang, M. Kula, W. Lu, Y. Luo, *Nano Lett.* **2005**, *5*, 1551-1555.
18 M. Grobis, K. H. Khoo, R. Yamachika, X. H. Lu, K. Nagaoka, S. G. Louie, M. F. Crommie, H. Kato, H. Shinohara, *Phys. Rev. Lett.* **2005**, *94*, 136802(1)-136802(4).
19 C. F. Hirjibehedin, C. P. Lutz, A. J. Heinrich, *Science*, **2006**, *312*, 1021-1024.
20 M. Kula, J. Jiang, W. Lu, Y. Luo, *J. Chem. Phys.* **2008**, *128*, 064705(1)-064705(7).
21 M. Paulsson, T. Frederiksen, M. Brandbyge, *Nano Lett.* **2006**, *6*, 258–262.
22 J. Lykkebo, A. Gagliardi, A. Pecchia, G. C. Solomon, *ACS Nano* **2013**, *7*, 9183–9194.
23 M. Paulsson, T. Frederiksen, H. Ueba, N. Lorente, M. Brandbyge, *Phys. Rev. Lett.* **2008**, *100*, 226604(1)-226604(4).
24 A. Troisi, M. A. Ratner, *Nano Lett.* **2006**, *6*, 1784–1788.
25 G. C. Solomon, A. Gagliardi, A. Pecchia, T. Frauenheim, A. D. Carlo, J. R. Reimers, N. S. Hush, *J. Chem. Phys.* **2006**, *124*, 094704()1–094704(10).
26 A. D. Becke, *J Chem. Phys.* **1993**, *98*, 5648-5652.
27 C. Lee, W. Yang, R. G. Parr, *Phys. Rev. B* **1988**, *37*, 785-789.
28 J. Jiang, C. K. Wang, L. Yi, Quantum chemistry for molecular electronics, QCME-V1.1.
29 C. K. Wang, Y. Luo, *J Chem. Phys.* **2003**, *119*, 4923-4928.
30 J. Jiang, M. Kula, Y. Luo, *J. Chem. Phys.* **2006**, *124*, 034708(1)-034708(10).
31 A. Troisi, M. A. Ratner, A. Nitzan, *J. Chem. Phys.* **2003**, *118*, 6072-6082.
32 M. Galperin, M. A. Ratner, A. Nitzan, *J. Phys.: Condens. Matter* **2007**, *19*, 103201.
33 Z. L. Ding, J. Jiang, H. B. Shu, X. S. Chen, W. Lu, *J. Nanosci. & Nanotech.* **2011**, *11*, 1-4.
34 A. Gagliardi, G. Romano, A. Pecchia, A. D. Carlo, T. Frauenheim, T. A. Niehaus, *New Journal of Physics* **2008**, *10*, 065020.